Construction and Building Materials 368 (2023) 130432

Contents lists available at ScienceDirect

Construction and Building Materials

journal homepage: www.elsevier.com/locate/conbuildmat

Confinement of concrete with FRCM: Influence of bond aspects under cyclic axial loading

Klajdi Toska [a,b], Flora Faleschini [c,*], Mariano Angelo Zanini [c]

[a] Laboratoire de Mécanique & Matériaux du Génie Civil – L2MGC, CY Cergy Paris Université, 5 Mail Gay Lussac, 95000 Neuville-sur-Oise, France
[b] CY Institute for Advanced Studies, 1 Rue Descartes, 95000 Neuville-sur-Oise, France
[c] Department of Civil, Environmental and Architectural Engineering, University of Padova, via Francesco Marzolo 9, Padova, Italy

ARTICLE INFO

Keywords:
Carbon fibers
FRCM
Concrete confinement
Bond
Cyclic loading
Stress–strain

ABSTRACT

Bond aspects may significantly influence the effectiveness of Fiber Reinforced Cementitious Matrix (FRCM) jackets as confining system. Among them, this paper focuses on the following variables: the overlapping length, the equivalent thickness of the fibers (directly related with the fabric weight), fibers coating presence (pre-impregnated with epoxy resin or fluid cement paste), and lastly, the reinforcement configuration (continuous or discontinuous layers). For this scope, an experimental campaign was carried out on cylindric specimens, subject to cyclic axial loading, strengthened with two layers of carbon-based FRCM (CFRCM). Failure modes, axial stress–strain curve, strength and stiffness deterioration and, lastly, plastic strains were analyzed. Experimental results indicate a clear effect of the investigated parameters on the overall effectiveness of the confining jackets: the best results were obtained when carbon fibers are epoxy-coated, recalling that for making the application feasible, a relatively large mesh size and a low degree of coating impregnation should be used for the textiles. Lastly, new relationships to predict the main parameters that define the cyclic behavior of confined concrete are proposed and compared with those found in literature for other confining systems (based on fiber-reinforced polymer FRP and transverse steel).

1. Introduction

Concrete confinement through external bonded reinforcement (EBR) can be achieved using different jacketing systems, and among them, in the last years the use of Fiber Reinforced Cementitious Matrix (FRCM) has significantly increased the attention of designers due to some interesting features of this composite. Indeed, compared to the most well-known Fiber Reinforced Polymer (FRP) solution, some benefits can be achieved, namely the avoidance of using large amounts of epoxy resins that have high cost, deteriorate when exposed to medium–high temperature (typically, higher than 70–80 °C), and have few compatibilities with cement-based materials, especially when wet surfaces are present [1]. Although, it is well-known that the FRCM strengthening systems behave differently from FRP, with the main evidence of performing worse in terms of strength enhancement. This behavior was well documented in literature e.g., by Triantafillou et al. [2], who compared the confining effectiveness of FRP and FRCM jackets with the same stiffness and strength. Such difference is based on the intrinsic characteristic of the FRCM system: in fact, FRCM presents multiple interfaces where bond stresses develop, i.e., one between the fibers and the matrix (the inorganic constituent of the composite), and one between the composite and the substrate to be strengthened or repaired. Thus, the maximum strength, the failure mode and, more generally the evolution of the stresses and strains in the FRCM-reinforced member differ significantly from that of FRP-counterparts. This is clearly visible comparing the stress–strain curve of FRCM and FRP in tension: the former typically exhibits a tri-linear curve (when clamping test setup is used [3]), whereas the latter a linear elastic behavior until failure. The FRCM stiffness changes during the tensile test [4], after the loss of the perfect bond present in the first elastic stage only, due to the following co-causes: (i) the multiple cracking and the redistribution of the stresses along the test sample after the first cracking stage; (ii) the propagation of the cracks along the sample; and (iii) the tension stiffening effect.

Bond behavior dominates, for many reasons, the overall performance of FRCM strengthening systems, independently from the configuration in which they are applied. When testing bond between FRCM and concrete substrate, different test methods were applied by each author, but mainly single [5] and double lap-shear tests [6] should be mentioned,

* Corresponding author.
E-mail address: flora.faleschini@dicea.unipd.it (F. Faleschini).

https://doi.org/10.1016/j.conbuildmat.2023.130432
Received 6 October 2022; Received in revised form 12 January 2023; Accepted 15 January 2023
Available online 25 January 2023

Table 1
Specimens' features.

Specimen group	Confinement	l_b (mm)	t_f (mm)	Condition	Layers	N. specimens
REF	–	–	–	–	–	3
C200_1D_C	CFRCM	200	0.047	Dry	2-continuous	3
C200_2D_C	CFRCM	200	0.061	Dry	2-continuous	3
C200_1D_D	CFRCM	200*	0.047	Dry	2-discontinuous	3
C300_1D_C	CFRCM	300	0.047	Dry	2-continuous	3
C200_1ER_C	CFRCM	200	0.047	Pre-impregnated (Epoxy Resin)	2-continuous	3
C200_1FC_C	CFRCM	200	0.047	Pre-impregnated (Fluid cement matrix)	2-continuous	2

* For each layer.

for their wide-spread diffusion. According to a large and well-established literature, the parameters that influence bond between FRCM and concrete can be summarized as: fiber types [7]; the presence or not of fibers coating [8], and its degree of impregnation [9]; the quality of the substrate and its preparation in terms of roughness [10]; the bond length [11]; the number of fiber layers [12]; the loading rate [13]; some environmental conditions, e.g., high temperature [14], carbonation, freezing/thawing [15] or wetting/drying cycles [16], etc. All the cited parameters may have an influence on the effectiveness of the strengthening system, changing substantially the bond capacity. Thus, they impact on the failure mode that may occur. That can be, in order of efficiency, from the worst to the best: FRCM debonding from the substrate, along the interface or detaching a portion of concrete; slippage of the fibers through the mortar; failure of the fibers, achieving their tensile strength.

Particularly focusing on the adoption of FRCM jackets to confine concrete members, bond plays again a significant role, because the stresses are transferred from the axially loaded member to the EBR system properly by means of the bond acting through the different interfaces, namely concrete-to-matrix and fibers-to-matrix. This is macroscopically evident looking at the failure modes that may be achieved: first, debonding may occur close to the end of the lap, mainly as a result of an insufficient overlapping length or due to an incomplete textile impregnation by the mortar [2,17,18], displaying a visible major vertical crack; another possibility relates to the slippage of the fibers inside the matrix [17,19,20]; lastly, bond capacity can remain intact, and the failure occurs for the reaching of fibers tensile strength [21,22]. In this last case, circular-shaped cross-section members are more homogenously stressed, displaying high confining efficiency. Instead, the presence of sharp edges, even if rounded, determines high stress concentration with premature FRCM failure [22], particularly when steel longitudinal reinforcement is present, for the potential occurrence of buckling phenomena [23].

Confinement of concrete with FRCM jacket has been widely investigated in literature, both for bare [24,25] and reinforced concrete (RC) members [26–28] under axial and under horizontal loading [29,30]. Recent research from the same authors of this work investigated how the axial load, when cyclically applied, affects the stress–strain behavior of the FRCM-confined concrete [31]. Particularly, within the analyzed research variables, the cyclic response was identified as comparable to the monotonic one; however, loss of bond may affect the cyclic stress–strain response more than in the case of the monotonic one. Therefore, in this work, some variables affecting bond condition between CFRCM jackets (with carbon fibers) and concrete substrate are analyzed in cylindrical specimens subject to cyclic axial loading. Specifically, the following parameters are investigated: two overlapping lengths, namely 200 and 300 mm; two equivalent thickness of the fibers, being 0.047 and 0.061 mm; the treatment applied to the carbon fibers, which can be dry or pre-impregnated, rather with epoxy-coating or with fluid cement-based matrix; the type of reinforcement configuration, realized with continuous or discontinuous layers. The range of the first parameter is chosen according to the current knowledge: indeed, for CFRCM systems with mesh size of 10x10 mm and nominal thickness of 0.095 mm, it was found that the effective bond length is between 200 and 300 mm [1], thus similar results can be expected also in the present case. Instead, for the equivalent thickness, the two values were chosen based on the available products provided by the producer of the FRCM system. Concerning the condition of the fibers, i.e., dry or pre-impregnated, the choice aims to reproduce the two most used solutions in the market (dry and epoxy-impregnated) and a third alternative, that consisted in pre-impregnating the carbon mesh in a fluid cement-based matrix (cement impregnated), was also investigated. Lastly, the two reinforcement configurations (continuous and discontinuous layers) applicable in the practice are analyzed.

2. Experimental program

The experimental program deals with the realization and testing of 20 cylindrical specimens with diameter and height $d \times h = 150 \times 300$ mm, which nomenclature and features are listed in Table 1. Note that the specimens are grouped into seven categories, which contain in all cases three identical specimens, except for one group, in which only two specimens are present due to some testing problems. Table 1 summarizes the specimens group name, the overlapping length l_b, fibers equivalent thickness t_f, fibers condition, reinforcement configuration and the number of specimens within each group. Specimens are labelled with a nomenclature that consists of three parts. The first letter identifies the fiber material (C = carbon) while the number characterizes the overlapping length (i.e., $l_b = 200$ or 300 mm). The second part of the label indicates the fiber type and condition, being 1 for the fiber net with $t_f = 0.047$ mm, and 2 for $t_f = 0.061$ mm, whereas the letter D stands for dry, ER for epoxy-resin coating and FC for fluid-cement pre-impregnating. The final part shows whether the fiber layers were applied continuously (C) or discontinuously (D).

2.1. Materials and specimens realization

To cast the specimens, one single concrete batch was realized with medium–low strength. The choice aims to simulate the material properties of existing structures, where repair or strengthening interventions may be required. All the concrete specimens were cured in water at 20 ± 2 °C for 28 days, and then were strengthened with the CFRCM composite. Then, they were left curing for at least other 28 days covered by humid tissues and placed inside plastic bags at 20 ± 2 °C.

Concrete specimens were characterized in terms of compressive strength on six samples with $d \times h = 150 \times 300$ mm, following the EN 12390 series as test reference [32]. Tests were carried out after 28 days of curing. Results are given in terms of average (*ave.*) and standard deviation (*st. dev.*): $f_c = 22.45 \pm 0.5$ MPa. The indirect tensile test [33] and secant elastic modulus [34] were evaluated on three samples with $d \times h = 100 \times 200$ mm too at the same age, being $f_{ct} = 2.94 \pm 0.5$ MPa and $E_c = 23.43 \pm 1.41$ GPa.

To realize the EBR strengthening system, CFRCM composites constituted by a premixed thixotropic mortar, with pozzolanic and short fibers additions, and carbon bi-directional nets were used. Concerning the mortar, different batches were mixed during the strengthening

Table 2
Properties of dry carbon fibers (M = provided by the manufactures, on single wire; E = experimental, on one groove).

Fiber type	t_f (mm)	Condition	E_f (GPa)		f_f (MPa)		ε_f (%)	
			M	E	M	E	M	E
1	0.047	Dry	240	236.5 ± 12	4900	1215 ± 225	1.80	0.95 ± 0.14
2	0.061	Dry	240	230 ± 11.5	4900	1059 ± 53	1.80	0.73 ± 0.14

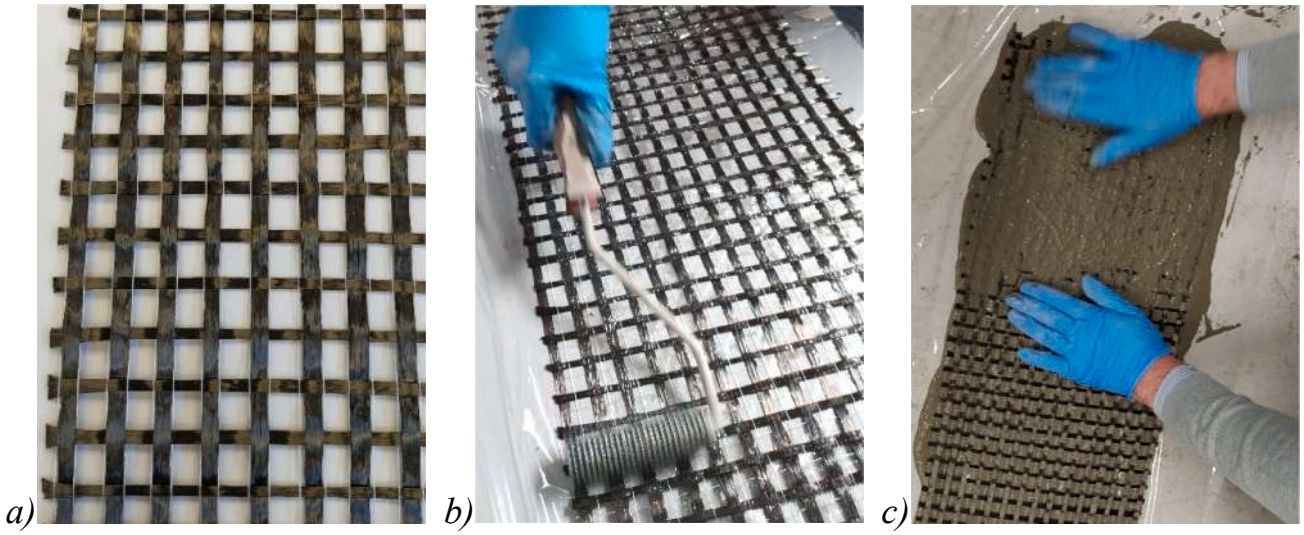

Fig. 1. A) dry fibers, b) epoxy resin and c) fluid cementitious matrix impregnation.

operations; for this reason, for each batch, three prismatic samples with 40 × 40 × 160 mm dimensions were realized and tested at 28 days to evaluate the compressive $f_{c,28}$ and flexural $f_{cf,28}$ strength according to [35]. However, both the properties were well stable, thus here the *ave.* and *st. dev.* values are given, only: $f_{c,28}$ = 23.1 ± 2.66 MPa and $f_{cf,28}$ = 5.05 ± 0.65 MPa.

Two types of dry carbon bi-directional nets were used: one with t_f = 0.047 mm and the other with t_f = 0.061 mm. For each type, fiber properties were tested on three specimens subject to uniaxial tensile tests [36], and which results are listed in Table 2. To realize the coated fibers, only the net with t_f = 0.047 mm was used: in one case it was pre-impregnated with epoxy resin, in the other with fluid cement. The epoxy resin was a thixotropic one with an elastic modulus of 4600 MPa, compression and flexural strength respectively 82 and 45 MPa. Concerning the second case, the impregnation procedure was performed just before applying the CFRCM jacket using a cementitious matrix with *w/b* ratio equal to 0.3 to obtain a fluid mixture. Fig. 1 shows the carbon fabric in dry conditions (a) and in epoxy resin (b) and fluid cementitious matrix impregnation (c).

Confinement operations were carried out after 28 days of curing, following the same protocol for all the specimens. To promote adherence between the concrete support and the FRCM jacket, and to prevent mortar moisture loss, specimens' surface was dumped with water just before applying the EBR system. Afterwards, a first layer of mortar (approximately 3–4 mm) was applied, followed by the first fiber layer, that was positioned gently pushing it onto the matrix. A second layer of mortar was applied and the same procedure was repeated for the second fiber layer, which was lastly covered with the mortar. The fiber was maintained slightly in tension by hand during its application, to avoid bubbles formation and imperfect contact. Overall, the thickness of the jackets did not exceed 10–12 mm. Note that the CFRCM jackets were applied leaving uncovered about 10 mm at the top and bottom of the cylinders, to ensure that the axial load is applied on the concrete core only, avoiding to stress the jacket axially. Lastly, after the strengthening procedure, specimens were covered with a humid tissue, closed in plastic bags and let curing until testing.

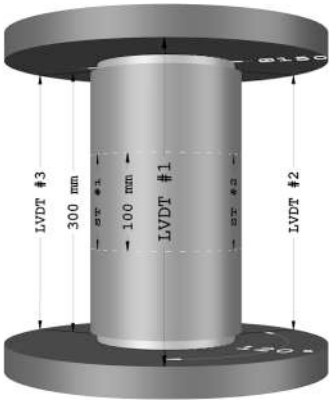

Fig. 2. Test setup.

2.2. Test set-up and loading protocol

Specimens were tested under the same loading protocol using a universal loading machine in a displacement control mode. The axial load was applied cyclically, with a displacement rate of 0.6 mm/min both for loading and unloading paths, similar than in [31]. The test was stopped when a significant strength reduction was observed, generally being lower than 50 % of the peak load. The cyclic loading was applied using single loading–unloading cycles, at increasing displacement steps. Before testing, the upper and bottom faces of the specimens were capped with high-strength mortar, to level the load application surface and ensure a proper distribution of the stresses within the sample. To prevent the specimens from moving during the test, a small compression (about 10 kN, corresponding to 0.56 MPa) was maintained constant during the unloading–reloading cycles.

Table 3
Results of unconfined specimens.

Specimen ID	f_{c0} (MPa)	ε_{c0} (%)	f_{cu} (MPa)	ε_{cu} (%)
REF1	22.95	0.33	18.36	0.46
REF2	21.92	0.27	17.54	0.34
REF3	22.47	0.31	17.98	0.41
REF ave.	22.45	0.30	17.95	0.40
REF st. dev.	0.52	0.03	0.58	0.06

The axial load was acquired continuously during the test, using the 600 kN load cell of the universal testing machine. Axial strains were monitored using three linear voltage displacement transducers (LVDTs), that acquired the displacement between the top and bottom plates and three strain transducers (STs), with a gauge length of 100 mm, applied directly onto the surface of the specimen. Note that STs were used to monitor small axial strains in the pre-peak branch, while the LVDTs to record the strains in the post-peak branch of the axial stress–strain curve. Both LVDTs and STs were installed equally spaced at 120° and their disposition is shown in Fig. 2.

3. Results and discussion

Tables 3 and 4 summarize the main experimental results for each sample tested, respectively for the unconfined and jacketed concretes. For the unconfined specimens, the peak axial strength f_{c0} and strain ε_{c0}, ultimate axial strength f_{cu} and strain ε_{cu} are listed. Ultimate conditions are evaluated, conventionally, when the load drops below the 80 % of the peak (Fig. 3a). Instead, for the CFRCM-confined specimens, first confined axial strength f_{cc} and strain ε_{cc}, ultimate confined axial strength f_{ccu} and strain ε_{ccu} are listed. In this case, as discussed thoroughly by the same authors in [31], the ultimate condition depends significantly on the type of stress–strain curve exhibited by the specimens after the first peak, which may be purely softening, softening with a further plateau or with hardening (see Fig. 3b). Particularly, Fig. 3b shows the multi-stage behavior of the FRCM-confined concrete, and it identifies the couples of (ε_c, f_c) for each situation:

- stage 1 is characterized by the same slope of the unconfined concrete;
- stage 2 is developed after the exceedance of f_{c0}, when the FRCM jacket is activated by the dilation of the concrete core until reaching f_{cc};
- stage 3 depends on the efficiency of the confinement, and this branch defines the ultimate conditions, too. The confining pressure exerted by the FRCM jacket may allow the specimen to increase (stage 3c) or maintain (stage 3b) the bearing capacity at increasing axial strains; alternatively, the confining pressure is not sufficient to sustain the load (stage 3a), which decreases with the increase of the axial strain.

Other than the above parameters, the strength enhancement at the first peak (f_{cc}/f_{c0}) and at the ultimate conditions (f_{ccu}/f_{c0}) compared to the unconfined strength are reported. Lastly, as a ductility index, the ratio of the axial strain at failure over that at the peak is shown ($\varepsilon_{ccu}/\varepsilon_{cc}$).

3.1. Failure mode

Most confined specimens showed similar cracking patterns which are visible in Fig. 4. Small vertical cracks appeared in the FRCM confining jacket when the loading history was near the first peak. Generally, specimens displayed a quite homogeneous and uniform vertical crack pattern and larger cracks were observed in the upper part of the elements. After ultimate load is reached, very few new crack openings were observed and failure was reached with the continuous openings of few of the existing main cracks. The main failure crack is generally near the overlapping start or end of the fabric layer, highlighting the failure due to fiber slippage in the matrix. Clear fiber rupture was observed only in the specimens with impregnated fibers, as can be seen in Fig. 4f and Fig. 4h. For specimens confined with epoxy-resin impregnated fibers, the spalling of the external mortar layer was observed (Fig. 4f). This is mainly due to a very dense vertical cracking pattern (Fig. 4e), generally at half height of the specimen, which eases the detachment of exterior mortar pieces.

Table 4
Results of confined specimens (in bold, the average value within each group is shown).

Specimen ID	f_{cc} (MPa)	ε_{cc} (%)	f_{ccu} (MPa)	ε_{ccu} (%)	f_{cc} / f_{c0}	f_{ccu} / f_{c0}	ε_{ccu} / ε_{cc}
C200_1D_C1	27.11	0.30	23.62	0.78	1.208	1.052	2.600
C200_1D_C2	26.82	0.28	22.29	0.74	1.195	0.993	2.643
C200_1D_C3	26.21	0.29	21.69	0.76	1.167	0.966	2.621
C200_1D ave.	**26.71**	**0.29**	**22.53**	**0.76**	**1.190**	**1.004**	**2.621**
C200_1D dev. st.	0.46	0.01	0.99	0.02	0.020	0.044	0.021
C200_2D_C1	27.05	0.24	21.23	0.76	1.205	0.946	3.167
C200_2D_C2	25.08	0.28	22.65	0.78	1.117	1.009	2.786
C200_2D_C3	27.36	0.28	23.92	0.86	1.219	1.065	3.071
C200_2D ave.	**26.50**	**0.27**	**22.60**	**0.80**	**1.180**	**1.007**	**3.008**
C200_2D st. dev.	1.24	0.02	1.35	0.05	0.055	0.060	0.198
C200_1D_D1	27.34	0.30	23.50	0.69	1.218	1.047	2.300
C200_1D_D2	28.56	0.35	23.58	0.72	1.272	1.050	2.057
C200_1D_D3	26.46	0.29	18.61	0.74	1.179	0.829	2.552
C200_1D ave.	**27.45**	**0.31**	**21.90**	**0.72**	**1.223**	**0.975**	**2.303**
C200_1D st. dev.	1.05	0.03	2.85	0.03	0.047	0.127	0.247
C300_1D_C1	26.57	0.32	24.45	0.80	1.184	1.089	2.500
C300_1D_C2	25.79	0.29	20.8	0.75	1.149	0.927	2.586
C300_1D_C3	26.40	0.28	22.61	0.77	1.176	1.007	2.750
C300_1D ave.	**26.25**	**0.30**	**22.62**	**0.77**	**1.169**	**1.008**	**2.612**
C300_1D st. dev.	0.41	0.02	1.83	0.03	0.018	0.081	0.127
C200_1ER_C1	27.48	0.27	28.78	1.05	1.224	1.282	3.889
C200_1ER_C2	27.64	0.26	28.81	1.14	1.231	1.283	4.385
C200_1ER_C3	27.56	0.37	25.54	1.12	1.228	1.138	3.027
C200_1ER ave.	**27.56**	**0.30**	**27.71**	**1.10**	**1.228**	**1.234**	**3.767**
C200_1ER st. dev.	0.08	0.06	1.88	0.05	0.004	0.084	0.687
C200_1FC_C1	26.45	0.28	23.64	0.77	1.178	1.053	2.750
C200_1FC_C2	26.74	0.29	24.25	0.81	1.191	1.080	2.793
C200_1FC_C ave.	**26.60**	**0.29**	**23.95**	**0.79**	**1.185**	**1.067**	**2.772**
C200_1FC_C st.dev.	0.21	0.01	0.43	0.03	0.009	0.019	0.030

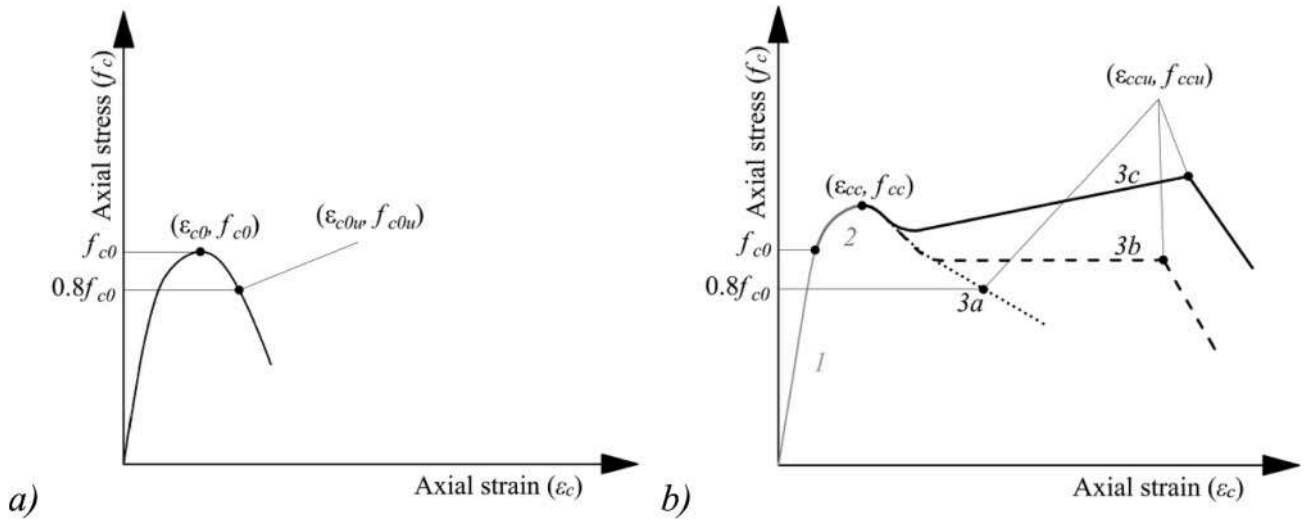

Fig. 3. Axial stress–strain behavior (envelope) and definition of the ultimate conditions for: a) unconfined concrete; b) FRCM-confined concrete.

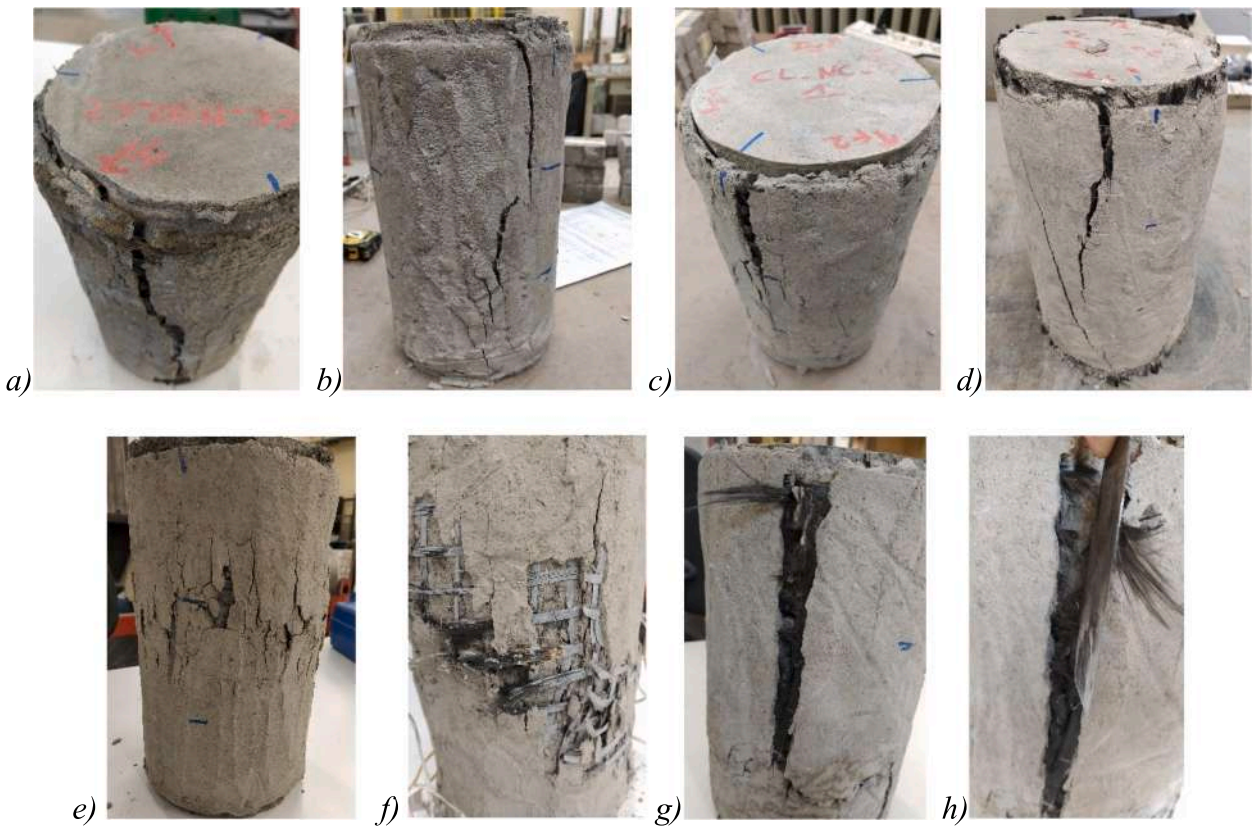

Fig. 4. Failure modes a) C200_1D_C, b) C200_2D_C, c) C200_1D_D, d) C300_1D_C, e-f) C200_1ER_C, g-h) C200_1FC_C.

3.2. Axial stress–strain behavior and bond parameters

Fig. 5(a–g) shows the experimental axial stress–strain curves for each category of specimens: black lines identify the envelope curves of each tested sample; red line represents the average envelope curve; the grey dotted line is the cyclic curve for one representative specimen within each category. Recall that a 10 mm unconfined space was left at the top and bottom of the specimens, in order to avoid axial loading of the FRCM jacket. Therefore, axial stresses are computed considering only the concrete cross-section area. Results are later discussed based on the following bond parameters: overlapping length (200 mm and 300 mm); continuous and discontinuous fiber layers; fabric weight (170 g/m^2 and 220 g/m^2) and fiber impregnation (with epoxy resin and fluid cement mortar) prior to confinement application.

3.2.1. Overlapping length

The overlapping length is an important parameter to prevent premature slippage of the fibers. Two overlapping lengths were considered in the present study: 200 mm and 300 mm. The first is based on previous research on bond between FRCM and concrete substrates, while the second is suggested from a literature review. In fact, Ombres [37] and D'Ambrisi et al. [38] investigated bond behavior in PBO FRCM –

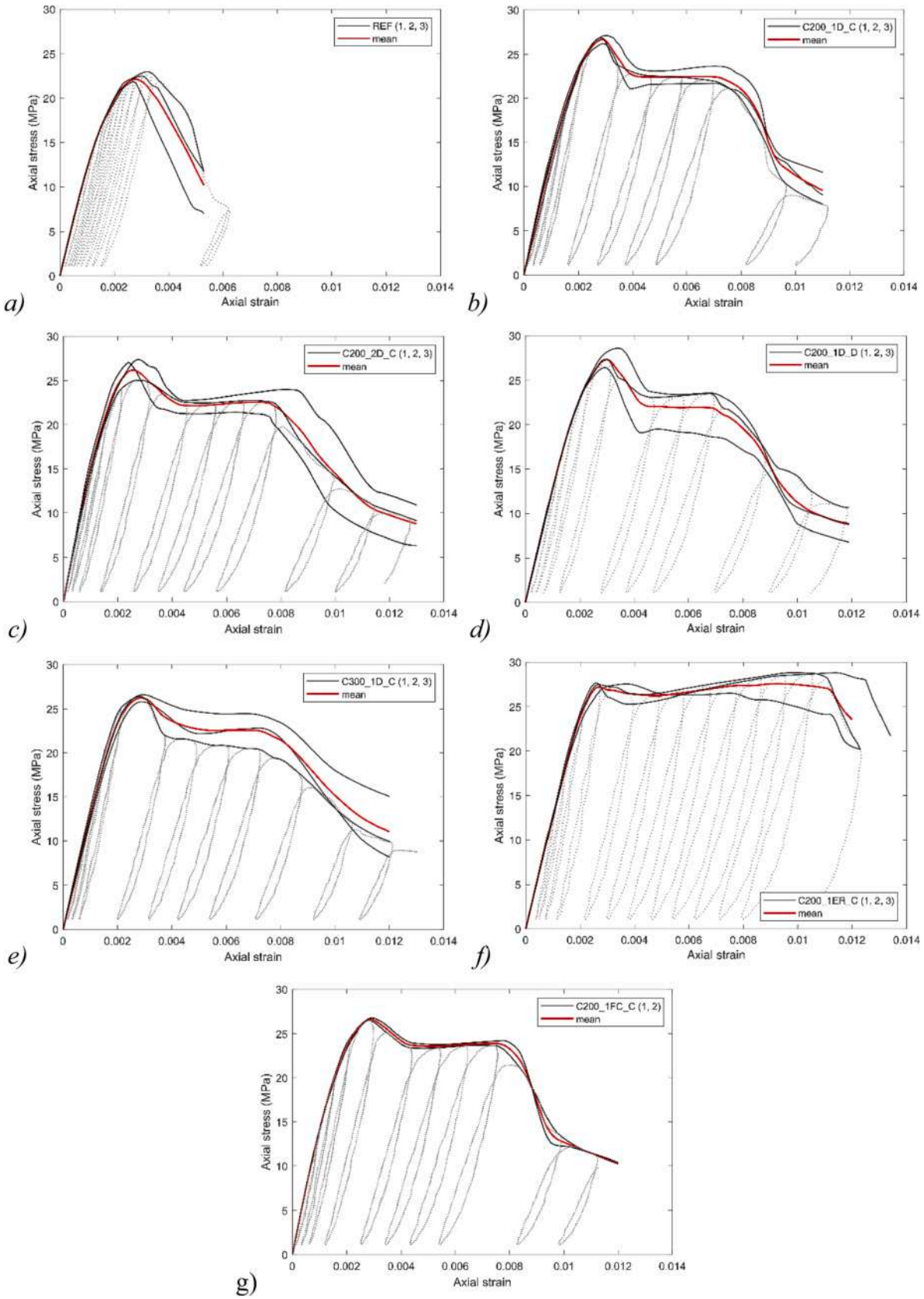

Fig. 5. Axial stress–strain curves of: a) REF; b) C200_1D_C; c) C200_2D_C; d) C200_1D_D; e) C300_1D_C; f) C200_1ER_C; g) C200_1FC_C specimens.

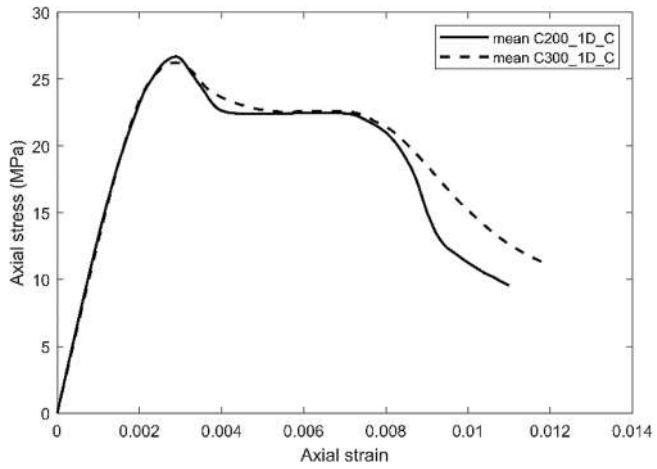

Fig. 6. Mean stress–strain curves of specimens with 200 and 300 mm overlapping length.

concrete systems, reporting an effective bond length ranging between 150 mm and 200 mm. Raof et al. [12] found that the effective bond length is in the range of 200–300 mm depending on the examined number of layers used. The Italian guidelines on the design of retrofitting interventions through FRCM composites [39] recommend an overlapping length of max (1/4 specimen's perimeter; 300 mm). Fig. 5b and 5e show respectively the axial stress–strain curves of specimens with an overlapping length of 200 and 300 mm while Fig. 6 compares the mean ones. Recall that the comparison shown in Fig. 6 refers to specimens characterized by the same features, which differentiate only per the overlapping length. Overall, the mean stress–strain curves do not show significant differences between the two categories, suggesting that 200 mm overlapping length is sufficient to prevent the jacket detachment. Results are slightly more scattered among the category with 300 mm overlapping length, than with 200 mm. In both cases, the first peak strength increases f_{cc}/f_{c0} are similar, being 19 % and 17 % respectively for 200 mm and 300 mm overlapping length. At the ultimate condition, for both the categories, the strength settles at the unconfined strength.

In the range of the analyzed variable, overlapping length seems to do not affect the ultimate strain and the overall ductility of the confined elements, too. Similar strains are observed at the first peak, with a difference of less than 0.01 %; the same applies at the ultimate condition. Consequently, almost identical axial ductility ($\varepsilon_{ccu}/\varepsilon_{cc}$) values are obtained for both specimens.

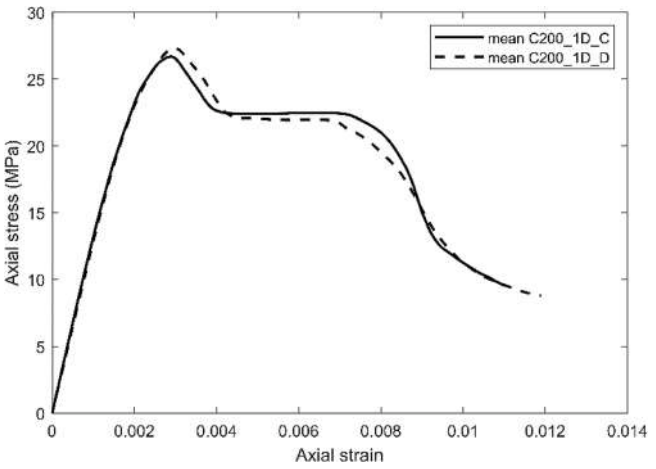

Fig. 8. Mean stress–strain curves of specimens confined with continuous and discontinuous layers.

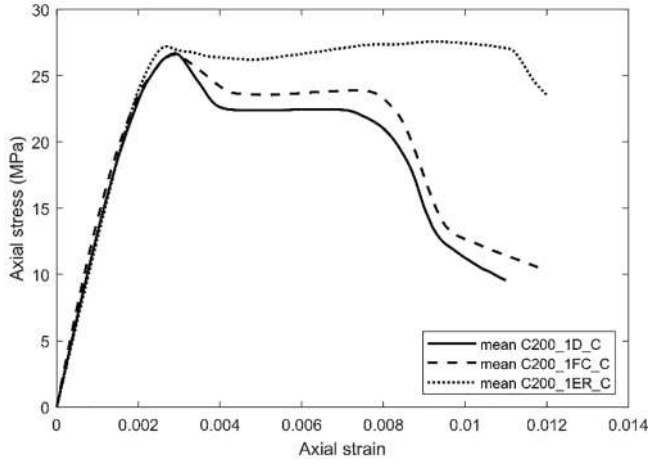

Fig. 9. Mean stress–strain curves of specimens confined with dry, fluid cement matrix and epoxy resin coated carbon fabric.

3.2.2. *Carbon fabric weight*

The fabric weight (i.e., the amount of carbon fibers present in the fabric) influences the nominal thickness and therefore the reinforcement amount of the overall FRCM system. Higher fabric weight should result in higher strength enhancements for the confined elements. However,

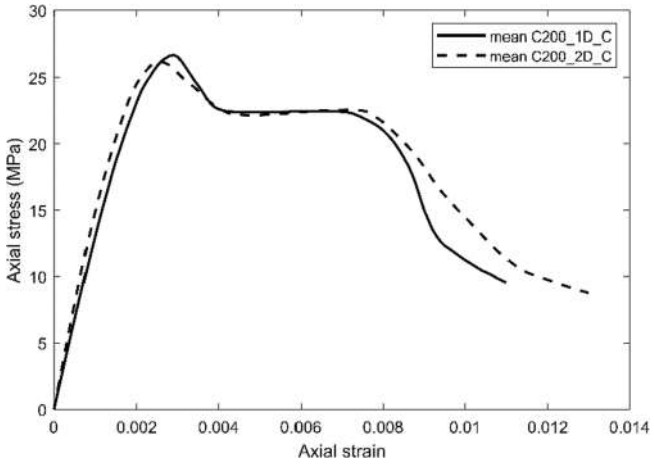

Fig. 7. Mean stress–strain curves of specimens confined with fabric weights of 170 g/m^2 and 220 g/m^2.

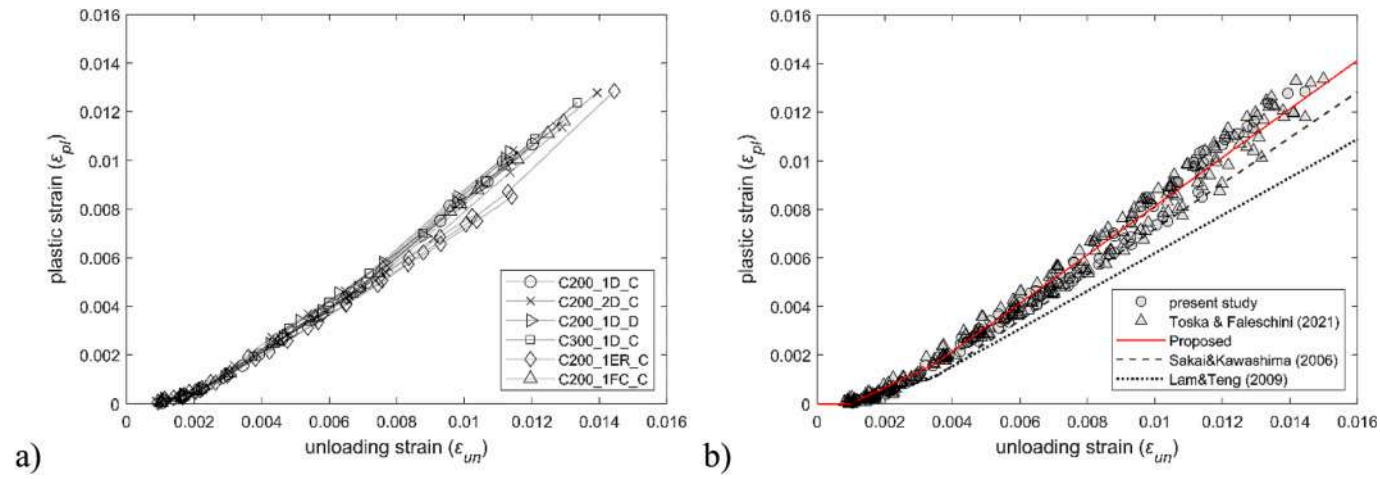

Fig. 10. Plastic vs unloading strain curves for different bond conditions (a) and the proposed correlation between ε_{un} and ε_{pl} (b).

due to fabric-matrix bond limits, it is not possible to linearly correlate the FRCM jacket confining capacity with this parameter. The results shown here confirm this statement, thanks to the comparison between the specimen categories realized with two fabric weights, 170 g/m^2 and 220 g/m^2, corresponding to 0.047 mm and 0.061 mm equivalent thickness, respectively. All the other variables are the same among the specimens. Their mean axial stress–strain curves are shown in Fig. 7, while peak and ultimate stress and strain values are listed in Table 4. Concerning the post-peak branch, they both display a stage 3b, maintaining an almost constant load close to the unconfined strength at increasing axial strains. Peak (f_{cc}) and ultimate (f_{ccu}) strength are similar in both cases, being 26.71 MPa vs 26.50 MPa, and 22.53 MPa vs 22.60 MPa, respectively for the 170 and 220 g/m^2 fabric. In terms of axial strains, the specimens with the heaviest fabric showed slightly lower axial strains at the first peak (0.27 % vs 0.29 %), and higher ones at ultimate point (0.80 % vs 0.76 %).

3.2.3. Continuous vs discontinuous layers

Wrapping concrete elements with FRCM composites can be carried out continuously (i.e., with one single carbon sheet) or discontinuously (i.e., one sheet for each layer). In the first case, there is a single overlapping zone at the end of the jacket, while in the second case two overlapping zones are present, one per each layer. Another difference relates the overall FRCM thickness of the intervention, being slightly higher in discontinuous applications due to the mortar application steps. Furthermore, care should be paid to ensure a sufficient offset of the overlapping zones among the different layers, to do not weak too much a single section.

Here, the results of these two categories of specimens are shown respectively in Fig. 5b and d, where the axial stress–strain curves are plotted respectively for the continuous and discontinuous method of application. Fig. 8 directly compares the mean stress–strain curves of the tested specimens for each case: the compared specimens differ only per the wrapping type. The overall behavior is again similar among the specimens of the two categories: all the specimens showed a 3b stage in the post-peak branch, maintaining a certain constant load after the first peak. In one case, a specimen realized with the discontinuous method displayed a steeper post-peak branch, resulting in a lower ultimate load (18.61 MPa) than the others (whose average is 23.50 MPa). Compared to the unconfined concrete, the first peak strength (f_{cc}) was enhanced by 22 % for the discontinuous and 19 % for the continuous method, while the axial strain at peak strength (ε_{cc}) was 0.31 % and 0.29 %, respectively for the two cases. Concerning the ultimate condition, f_{ccu} was respectively 21.90 and 22.53 MPa for discontinuous and continuous application, while slightly lower ultimate axial strains (ε_{ccu}) were recorded for the discontinuous method (0.72 % vs 0.76 %).

3.2.4. Fiber impregnation presence: epoxy resin vs cementitious matrix

Carbon fibers in commerce can be found dry or pre-impregnated. Generally, fiber impregnation is done through epoxy resins and can significantly enhance fiber–matrix bond and also promotes a more uniform stress distribution throughout the fibers present in a yarn. In the present investigation, apart from dry and epoxy-impregnated fibers, the effect of pre-impregnation using a fluid cement-based matrix was analyzed.

Axial stress–strain curves for the confined specimens with epoxy-impregnated (ER) and fluid cement matrix (FC) are shown in Fig. 5f and Fig. 5g, while specimens confined with dry fibers are shown in Fig. 5b. For sake of comparison, Fig. 9 shows the mean stress–strain curve of each case. It is clear that the epoxy-impregnation contribution to the FRCM confinement effectiveness appears very significant. The group of epoxy-impregnated is the only one, among the tested, which shows a clear hardening behavior after the first peak (stage 3c), recording higher strength values at ultimate conditions (f_{ccu}) and not at the first peak (f_{cc}). Similar results were achieved in [31] by the same authors with confined concrete with almost the same unconfined strength, strengthened with 4 layers of dry-CFRCM. Significant improvement was observed also in the axial strain capacity, with ultimate strain above 1 % recorded in all three tested specimens. At the first peak (f_{cc}, ε_{cc}), only slight differences were observed compared to the other considered cases, mainly in terms of strength (23 % more than the initial unconfined strength), while mean axial strain at the first peak was 0.30 %. ER specimens showed also the highest ductility ($\varepsilon_{ccu}/\varepsilon_{cc}$), being about 3.77, compared to the other analyzed cases where ductility varies between 2.62 and 2.77.

The specimens where the fabric was impregnated in a fluid cement matrix before their application are characterized by a less effectiveness than the epoxy-impregnated ones. However, similar strength levels were recorded in the first peak (26.60 MPa and 27.56 MPa, respectively for FC and ER specimens). In the post-peak branch, even though a slight hardening trend can be observed, the overall behavior is closer to a stage 3b trend rather than 3c. A part than the ER specimens, the FC impregnation was able to maintain the highest bearing capacity (about 24 MPa, 7 % higher than the unconfined strength) among specimens exhibiting a post-peak stage 3b.

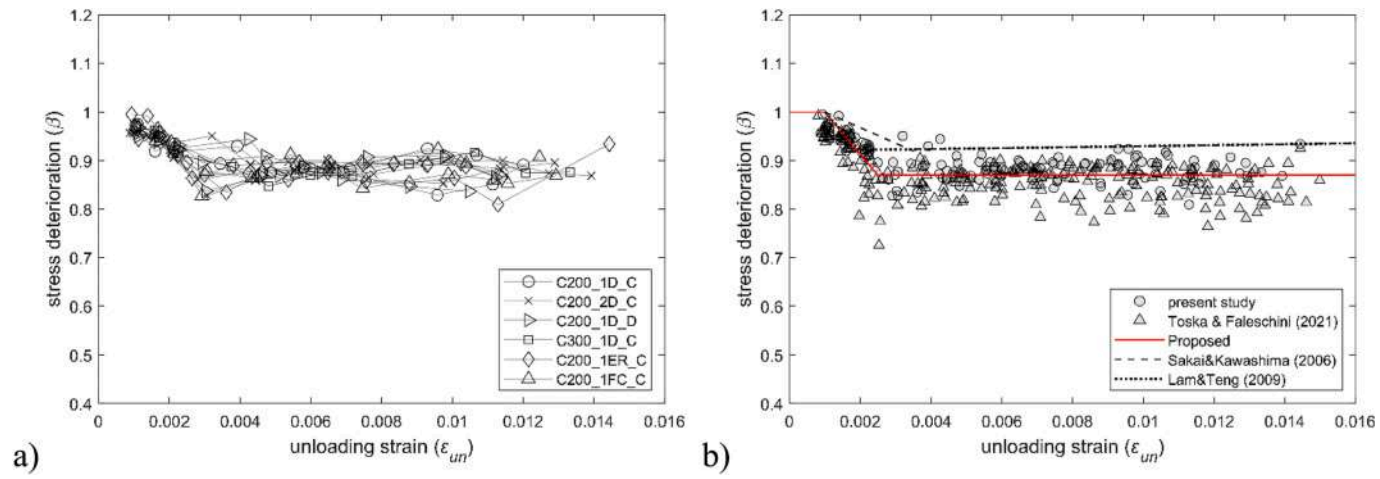

Fig. 11. Stress deterioration vs unloading strain curves for different bond conditions (a) and the proposed correlation between ε_{un} and β (b).

3.3. Hysteretic behavior of FRCM confined concrete

Previous research on steel and FRP confined concrete has shown that the stress–strain curve of specimens tested under monotonic compression corresponds to the envelope curve of specimens tested under cyclic compression load. Recently, Toska and Faleschini [31] demonstrated that the same applies also for FRCM confined concrete, independently of the fiber type, number of confining layers or specimens' cross-section shape. Some slight differences may apply in the post-peak branch, but they are generally negligible. In this section plastic strains, stress deterioration and stiffness deterioration for the envelope compression cycles of FRCM-confined concrete are presented. All the above parameters are directly related to the envelope unloading strain (ε_{un}). A more detailed explanation of the meaning of the variables listed below can be found in [31] and are graphically explained in the Annex.

3.3.1. Plastic strains

To investigate the effect of different bond conditions on plastic strains development during full compression cycles starting from the envelope curve, it is necessary to analyze the relation between unloading strains and residual plastic strains. In the present study, reloading started before the complete unloading of the specimens (a constant compression load was always maintained, see Section 2.2), therefore, plastic strains were not directly recorded. Since unloading paths are highly nonlinear when the curve approaches zero stresses, plastic strains were estimated from the recorded stress–strain curve by extending the unloading branch to the zero-stress point following the Lam and Teng's [40] proposed method for FRP confined concrete, which was previously used by [31] and [41] for FRCM confinement, too.

Plastic strains can be simply estimated as:

$$\varepsilon_{pl} = \varepsilon_{re} - \frac{f_{re}}{E_{un,0}} \tag{1}$$

where $E_{un,0}$ is the slope of the unloading path to zero, and can be estimated as:

$$E_{un,0} = min\begin{cases} \dfrac{0.5 \bullet f_{c0}}{\varepsilon_{un}} \\ \dfrac{f_{un}}{\varepsilon_{un} - \varepsilon_{pl}} \end{cases} \tag{2}$$

According to the authors, in almost all cases $E_{un,0}$ takes the value of $\frac{0.5 f_{c0}}{\varepsilon_{un}}$, while it can be evaluated with the second formulation when the unloading stress or strain is very small.

Fig. 10a shows the plastic vs unloading strain curves for all the tested specimens. It can be observed that the different bond conditions tested here have a negligible effect on plastic strains: all specimens display similar trend, with almost overlapping curves. Only the specimens made with the ER impregnation show slightly lower plastic strains compared to the others, for unloading strains higher than 0.008. The difference, however, can be considered irrelevant. Previously the same authors experimentally showed that the number of FRCM layers, fiber material and cross-section shape have little influence on the recorded plastic strain values. Similar results were also obtained for FRP confined concrete subject to cyclic loading [42–45].

When dealing with steel confined concrete, Sakai and Kawashima [43] distinguished two plastic strain regions, one for $0.001 < \varepsilon_{un} < 0.0035$ and another for $\varepsilon_{un} > 0.0035$, proposing a linear relationship between ε_{un} and ε_{pl} for each of them. For FRP confined elements, Lam and Teng [40] assumed in their model the same two regions, but proposed a different relationship considering also the dependence of plastic strains on the unconfined concrete strength. For $\varepsilon_{un} < 0.001$, plastic strains (ε_{pl}) are assumed instead null. However, both proposals do not well describe the experimental data for FRCM confined concrete, as shown in Fig. 10b. In this figure, data collected from the present study and from [31] are plotted together, and the two above-mentioned models are applied to this dataset. The dashed and dotted line are used to represent respectively Sakai and Kawashima [43] and Lam and Teng [40] models.

Looking at the experimental observations for plastic strains of FRCM confined concrete plotted in Fig. 10b, it is possible to distinguish again three main regions, i.e. $\varepsilon_{un} < 0.001, 0.001 < \varepsilon_{un} < 0.0035$ and $\varepsilon_{un} > 0.0035$. According to these data, the following relationships are proposed here to predict plastic strains in FRCM confined concrete:

$$\varepsilon_{pl} = \begin{cases} 0 & \varepsilon_{un} \le 0.001 \\ 0.652(\varepsilon_{un} - 0.001) & 0.001 \le \varepsilon_{un} \le 0.0035 \\ \varepsilon_{un} - 0.0019 & \varepsilon_{un} \ge 0.0035 \end{cases} \tag{3}$$

The above relations are based first on fitting the results in the region $\varepsilon_{un} \ge 0.0035$, and then ensuring the continuity of the function within the range $0.001 \le \varepsilon_{un} \le 0.0035$, which is obtained connecting the two known points for $\varepsilon_{un} = 0.001$ and $\varepsilon_{un} = 0.0035$. The coefficients of determination for Equation (3) are 0.85 within the range of $0.001 \le \varepsilon_{un} \le 0.0035$, and 0.98 for $\varepsilon_{un} \ge 0.0035$. The goodness of fit of Equation (3) can be observed also graphically in Fig. 10b, where the proposed relationships are shown with the red solid line and are

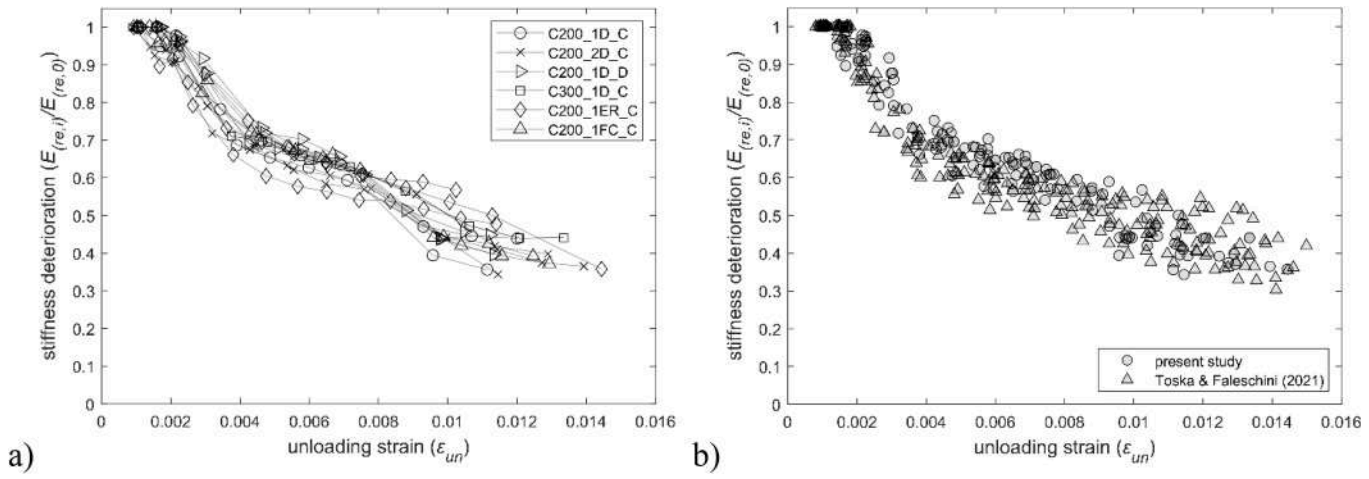

Fig. 12. Stiffness deterioration vs unloading strain curves for different bond conditions (a) and comparison with stiffness deterioration data from [31] (b).

compared to the Sakai and Kawashima [43] and Lam and Teng models [40].

3.3.2. Stress deterioration

This section investigates the relationship between the unloading strain and the new stress on a following reloading branch, when reaching the envelope unloading strain. The new reloading stress (f_{new}) is generally lower than the unloading one (f_{un}) from the envelope curve, due to stress deterioration occurring after cyclic loading in the post-peak branch. To describe this phenomenon, a stress deterioration ratio β is defined following a general expression given by:

$$\beta = \frac{f_{new}}{f_{un}} \tag{4}$$

where f_{un} is the envelope unloading stress and f_{new} is the new stress in the reloading path corresponding to the initial unloading strain from the envelope curve. More details and graphical explanation on the parameters can be found in [31] and are graphically represented in the Annex.

Fig. 11a shows stress deterioration (β) vs unloading strain (ε_{un}) for all the specimens tested in this experimental campaign. It can be observed that the different bond conditions analyzed here have a little influence in the stress deterioration due to cyclic loading. In fact, similar trends are observed for all specimens. For small unloading strain values, stress deterioration is very small, with β values very close to the unit. As unloading strains increase, β value decreases almost linearly and stabilizes at values between 0.9 and 0.85. Similar results were obtained also in [31], for different confining layers, fiber materials and cross-section shape, as can be seen in Fig. 7b, which plots the overall dataset from the two works.

Previous studies on FRP confined concrete showed that the ratio of the new stress f_{new} in a reloading path over the envelope unloading one f_{un} is independent on the unloading strain (ε_{un}), after a certain value of ε_{un}. The experimental results obtained by Lam et al. [42] included data with $\varepsilon_{un} > 0.002$ only, and showed an average β value of 0.916 (with *st. dev.* $= 0.006$). Shao et al. [46] suggested a constant ratio of $\beta = 0.9$ after the bend point in the stress–strain curve based on compressive cyclic tests on FRP-confined cylinders. As for the plastic strains, Lam & Teng [40] and Sakai and Kawashima [43] identify-three different intervals in the unloading strains domain, for FRP confined elements and steel confined ones, respectively. In the first region, for $\varepsilon_{un} \leq 0.001$, both of them consider stress deterioration insignificant, assuming $\beta = 1$. The intermediate interval is taken between $\varepsilon_{un} = 0.001$ and $\varepsilon_{un} = 0.002$ for [40], and between $\varepsilon_{un} = 0.001$ and $\varepsilon_{un} = 0.0035$ for [43], assuming in both cases a linear decreasing trend. The last region applies for $\varepsilon_{un} \geq 0.002$ and $\varepsilon_{un} \geq 0.0035$ respectively for [40] and [43], and here a constant function with $\beta = 0.92$ is proposed by both authors. However, again, the two proposals do not describe well the data for the FRCM confinement, where stress deterioration results slightly higher than for FRP confinement. The following equation is then proposed on the basis of the same assumptions carried out by the other authors [40,43], aiming at achieving a best fitting to the experimental results collected from FRCM confined concrete subjected to cyclic loading:

$$\beta = \begin{cases} 1 & \varepsilon_{un} \leq 0.001 \\ 1 - 86.76(\varepsilon_{un} - 0.001) & 0.001 \leq \varepsilon_{un} \leq 0.0025 \\ 0.87 & \varepsilon_{un} \geq 0.0025 \end{cases} \tag{5}$$

The standard deviation for $\varepsilon_{un} \geq 0.0025$ is 0.03. The intermediate linear function (for $0.001 \leq \varepsilon_{un} \leq 0.0025$) is determined by connecting the two known points at $\varepsilon_{un} = 0.001$ and 0.0025. The results of the Eq. (5) are shown with the red solid line in Fig. 11b.

3.3.3. Reloading elastic modulus E_{re}

Cyclic loading history reduces the initial elastic modulus of concrete. Even though some softening phenomena can be observed during reloading, generally, this reduction is considered and modeled as a linear curve, at least up to the initial envelope unloading strain (ε_{un}) [40,46]. Due to internal cracks and damage accumulation, during the reloading paths concrete does not return to the unloading stress when it reaches the unloading strain, but it achieves a lower stress value, f_{new}. After this point ($\varepsilon_{un}, f_{new}$), the trend gets highly nonlinear and can be approximated with a parabolic curve.

The linear part of the reloading path can be defined by the reloading slope E_{re} as follows:

$$E_{re} = \frac{f_{new} - f_{re}}{\varepsilon_{un} - \varepsilon_{re}} \tag{6}$$

which is also graphically represented in the Annex.

To evaluate the stiffness deterioration due to cyclic loading, it is necessary to calculate the ratio of the reloading slope at the i-th cycle $E_{re,i}$ over the reloading slope at the first cycle $E_{re,0}$. Note that if the first unloading strain is small enough, $E_{re,0}$ is generally equal to the initial elastic modulus of the concrete.

Fig. 12a compares stiffness deterioration ($E_{re,i}/E_{re,0}$) trends for the different bond conditions considered in this study. No significant

differences can be observed within the set of the tested samples. All curves show a very low, almost null, deterioration for small unloading strains ($\varepsilon_{un} < 0.002$). When axial strain exceeds 0.002, concrete turns out from the initial elastic behavior; then, internal cracking and damage accumulation lead to a fast and almost linear stiffness deterioration. When axial strain exceeds 0.004, the FRCM confining jacket is fully activated and is able to slow down the initial fast stiffness loss that is recorded near the peak strength. The linear descending trend of the reloading stiffness continues during all the cyclic loading history, but at a slower rate for $\varepsilon_{un} > 0.004$. Very similar results were obtained also in [31], where no significant differences in terms of stiffness deterioration were observed comparing specimens realized with a different number of confining layers, material and cross-section shapes. The results are compared to the present ones in Fig. 12b.

4. Conclusions

The experimental campaign presented in this paper aimed to investigate the influence of different bond conditions on FRCM confined concrete subject to compressive cyclic loading. The following parameters are investigated: two overlapping lengths (200 and 300 mm); two equivalent thickness of the fibers (0.047 and 0.061 mm); the treatment applied to the carbon fibers, (dry or pre-impregnated, rather with epoxy-resin (ER) or with fluid cement-based matrix (FC)) and reinforcement configuration (continuous or discontinuous layers). Overall, the results identified that the pre-impregnation of the fibers and the method for layers application (continuous and discontinuous) have the major impacts on the overall response of the specimens under cyclic axial loading. More specifically, the experimental results showed that:

- with exception of the epoxy-resin pre-impregnated specimens, which showed a clear hardening behavior (stage-3a), the other tested specimens showed similar axial stress–strain curves, independently of the bond conditions, showing a stage-3b in the post-peak behavior;
- the gain in the first confined peak strength (f_{cc}) over the unconfined strength is little influenced by the parameters investigated here, and varies between 17 % (300 mm overlapping length) and 23 % (epoxy-resin pre-impregnated fibers);
- the first peak strain for confined elements (ε_{cc}) ranges between 0.27 % and 0.31 %, being very similar to the unconfined peak strain (ε_{c0}), that has a mean value of 0.3 %.
- the ultimate confined peak strength (f_{ccu}), evaluated at 20 % of the peak load drop, was equal to the unconfined strength (f_{c0}) in all the specimens, except for specimens with pre-impregnated fibers, where f_{ccu} was 7 % and 23 % higher, for FC and ER specimens, respectively;
- specimens with discontinuous applied layers showed the lowest axial ductility ($\varepsilon_{ccu}/\varepsilon_{cc}$), being 2.3, while ER ones showed the highest axial ductility, being 3.77. Other specimens showed similar ductility varying between 2.6 and 3;
- the analyzed bond conditions used in the tested FRCM confining jackets have little influence on the parameters defining unloading and reloading paths (i.e., plastic strains, stress and stiffness deterioration) during cyclic loading;
- existing formulations calibrated on FRP confined concrete do not accurately predict plastic strains and stress deterioration for FRCM-confined concrete. Based on the present experimental data and on previous ones reported in [31], new formulations, consistent with the experimental observations, are proposed.

CRediT authorship contribution statement

Klajdi Toska: Conceptualization, Data curation, Investigation, Formal analysis, Visualization. **Flora Faleschini:** Conceptualization, Methodology, Investigation, Resources, Supervision, Project administration. **Mariano Angelo Zanini:** Investigation, Validation, Project administration.

Declaration of Competing Interest

The authors declare that they have no known competing financial interests or personal relationships that could have appeared to influence the work reported in this paper.

Data availability

Data will be made available on request.

Acknowledgments

Authors would like to thank G&P Intech for providing the FRCM systems. Eng. Lucia Sambataro is also acknowledged for her help during specimens' preparation.

Appendix

Annex: Main parameters defining the unloading and reloading paths in the cyclic behavior of FRCM-confined concrete.

When dealing with cyclic behavior of confined concrete it is important to describe the unloading and reloading stress–strain paths during the loading history. Plastic strains (residual axial strain when concrete is unloaded to zero stress), stress and stiffness deterioration are essential parameters that define unloading and reloading paths. These parameters and others needed for their computation are graphically explained in Fig. A1.

Where:

f_{un} is the unloading stress from the envelope curve;
ε_{un} is the unloading strain from the envelope curve;
f_{re} is the reloading stress;
ε_{re} is the reloading strain;
ε_{pl} is the plastic strain at zero stress;
$E_{un,0}$ is the slope of the unloading path to zero;
f_{new} is the stress in the reloading path corresponding to the unloading axial strain from the envelope curve;
E_c is the initial stiffness of the concrete;
E_{re} is the slope of the reloading path.

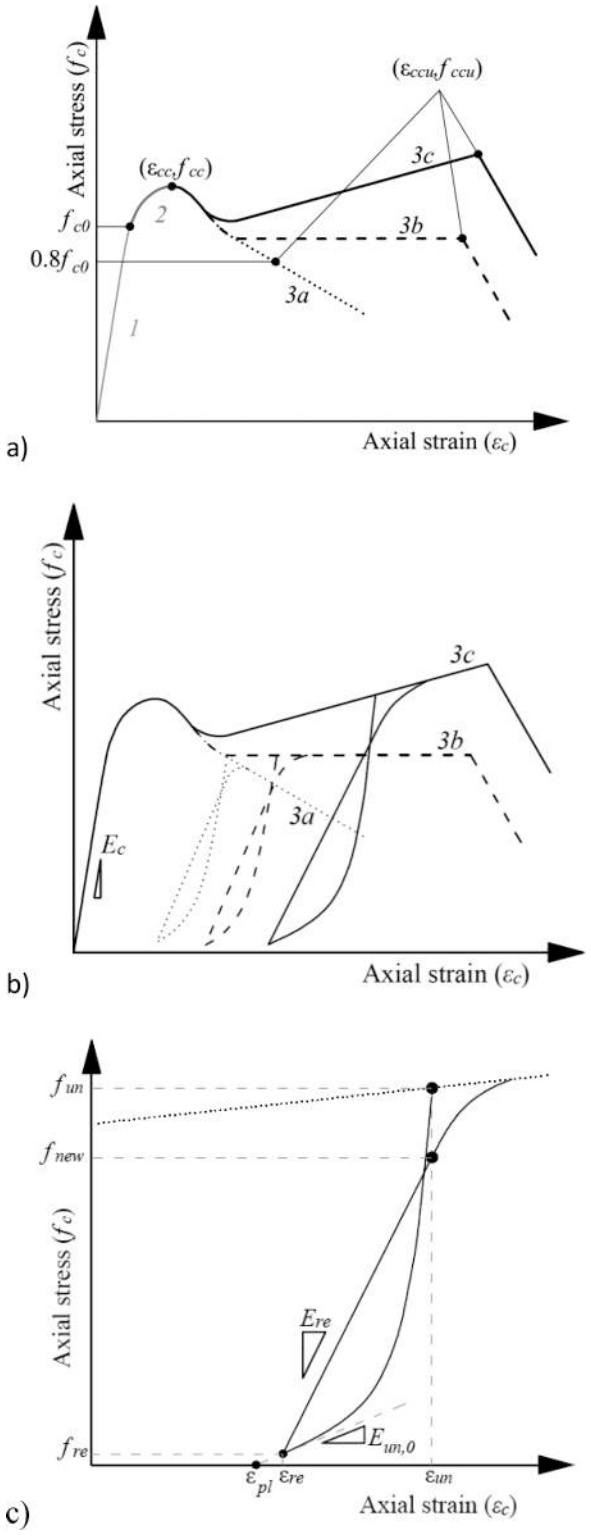

Fig. A1. Graphic representation of the main parameters of cyclic stress–strain curves of FRCM-confined concrete.

References

[1] L.N. Koutas, Z. Tetta, D.A. Bournas, T.C. Triantafillou, Strengthening of concrete structures with textile reinforced mortars: state-of-the-art review, Journal of Composites for Construction 23 (1) (2019) 03118001.

[2] T.C. Triantafillou, C.G. Papanicolaou, P. Zissimopoulos, T. Laourdekis, Concrete confinement with textile-reinforced mortar jackets, ACI structural journal 103 (1) (2006) 28.

[3] G.P. Lignola, C. Caggegi, F. Ceroni, S. De Santis, P. Krajewski, P.B. Lourenço, M. Morganti, C.(. Papanicolaou, C. Pellegrino, A. Prota, L. Zuccarino, Performance assessment of basalt FRCM for retrofit applications on masonry, Composites Part B: Engineering 128 (2017) 1–18.

[4] F. Nerilli, B. Ferracuti, A tension stiffening model for FRCM reinforcements calibrated by means of an extended database, Composite Structures 284 (2022) 115100.

[5] T. D'Antino, C. Carloni, L.H. Sneed, C. Pellegrino, Matrix–fiber bond behavior in PBO FRCM composites: A fracture mechanics approach, Engineering Fracture Mechanics 117 (2014) 94–111.

[6] L.H. Sneed, T. D'Antino, C. Carloni, C. Pellegrino, A comparison of the bond behavior of PBO-FRCM composites determined by double-lap and single-lap shear tests, Cement and Concrete Composites 64 (2015) 37–48.
[7] A. Younis, U. Ebead, Bond characteristics of different FRCM systems, Construction and Building Materials 175 (2018) 610–620.
[8] D. Dvorkin, A. Poursaee, A. Peled, W.J. Weiss, Influence of bundle coating on the tensile behavior, bonding, cracking and fluid transport of fabric cement-based composites, Cement and Concrete Composites 42 (2013) 9–19.
[9] J. Donnini, V. Corinaldesi, A. Nanni, Mechanical properties of FRCM using carbon fabrics with different coating treatments, Composites Part B: Engineering 88 (2016) 220–228.
[10] T. D'Antino, L.H. Sneed, C. Carloni, C. Pellegrino, Influence of the substrate characteristics on the bond behavior of PBO FRCM-concrete joints, Construction and Building Materials 101 (2015) 838–850.
[11] A. Dalalbashi, B. Ghiassi, D.V. Oliveira, A. Freitas, Fiber-to-mortar bond behavior in TRM composites: effect of embedded length and fiber configuration, Composites Part B: Engineering 152 (2018) 43–57.
[12] S.M. Raoof, L.N. Koutas, D.A. Bournas, Bond between textile-reinforced mortar (TRM) and concrete substrates: Experimental investigation, Composites Part B: Engineering 98 (2016) 350–361.
[13] C. Carloni, S. Verre, L.H. Sneed, L. Ombres, Loading rate effect on the debonding phenomenon in fiber reinforced cementitious matrix-concrete joints, Composites Part B: Engineering 108 (2017) 301–314.
[14] S.M. Raoof, D.A. Bournas, Bond between TRM versus FRP composites and concrete at high temperatures, Composites Part B: Engineering 127 (2017) 150–165.
[15] P.D. Askouni, C.C.G. Papanicolaou, Residual TRM-to-Concrete Bond after Freeze-Thaw Cycles, Materials 14 (18) (2021) 5438.
[16] F. Ceroni, A. Bonati, V. Galimberti, A. Occhiuzzi, Effects of environmental conditioning on the bond behavior of FRP and FRCM systems applied to concrete elements, Journal of Engineering Mechanics 144 (1) (2018) 04017144.
[17] T. Trapko, K. Rogalski, M. Musiał, L. Ombres, Effectiveness of Concrete Elements Strengthening through PBO-FRCM Confinement with Various Types of Anchorage, Journal of Materials in Civil Engineering 33 (1) (2021) 04020409.
[18] G.E. Thermou, K. Katakalos, G. Manos, Concrete confinement with steel-reinforced grout jackets, Materials and Structures 48 (5) (2015) 1355–1376.
[19] A. Cascardi, F. Micelli, M.A. Aiello, FRCM-confined masonry columns: experimental investigation on the effect of the inorganic matrix properties, Construction and Building Materials 186 (2018) 811–825.
[20] D.A. Bournas, P.V. Lontou, C.G. Papanicolaou, T.C. Triantafillou, Textile-reinforced mortar versus fiber-reinforced polymer confinement in reinforced concrete columns, ACI Structural Journal 104 (6) (2007) 740.
[21] L. Ombres, S. Verre, Structural behaviour of fabric reinforced cementitious matrix (FRCM) strengthened concrete columns under eccentric loading, Composites Part B: Engineering 75 (2015) 235–249.
[22] J. Gonzalez-Libreros, M.A. Zanini, F. Faleschini, C. Pellegrino, Confinement of low-strength concrete with fiber reinforced cementitious matrix (FRCM) composites, Composites Part B: Engineering 177 (2019), 107407.
[23] K. Toska, F. Faleschini, M.A. Zanini, L. Hofer, C. Pellegrino, Repair of severely damaged RC columns through FRCM composites, Construction and Building Materials 273 (2021) 121739.
[24] F. Micelli, A. Cascardi, M.A. Aiello, Pre-Load Effect on CFRP-Confinement of Concrete Columns: Experimental and Theoretical Study, Crystals 11 (2) (2021) 177.
[25] A.H. Adheem, M.M.A. Kadhim, A. Jawdhari, A. Fam, Confinement model for concrete wrapped with fiber reinforced cementitious mortar, Construction and Building Materials 312 (2021) 125401.
[26] F. Faleschini, M.A. Zanini, L. Hofer, C. Pellegrino, Experimental behavior of reinforced concrete columns confined with carbon-FRCM composites, Construction and Building Materials 243 (2020) 118296.
[27] L. Ombres, S. Verre, FRCM confined reinforced concrete columns: Experimental behavior and modeling, ACI Special Publication 345 (2021) 102–116.
[28] F. Faleschini, M.A. Zanini, L. Hofer, K. Toska, D. De Domenico, C. Pellegrino, Confinement of reinforced concrete columns with glass fiber reinforced cementitious matrix jackets, Engineering Structures 218 (2020) 110847.
[29] M.A. Zanini, K. Toska, F. Faleschini, C. Pellegrino, Seismic reliability of reinforced concrete bridges subject to environmental deterioration and strengthened with FRCM composites, Soil Dynamics and Earthquake Engineering 136 (2020) 106224.
[30] K. Toska, L. Hofer, F. Faleschini, M.A. Zanini, C. Pellegrino, Seismic behavior of damaged RC columns repaired with FRCM composites, Engineering Structures 262 (2022) 114339.
[31] K. Toska, F. Faleschini, FRCM-confined concrete: Monotonic vs Cyclic axial loading, Composite Structures 268 (2021) 113931.
[32] En 12390–3., Testing hardened concrete - Part 3: Compressive strength of test specimens, Committee European de Normalisation, Brussels, Belgium, 2019.
[33] En 12390–6., Testing hardened concrete - Part 6: Tensile splitting strength of test specimen, Committee European de Normalisation, Brussels, Belgium, 2010.
[34] En 12390–13., Testing hardened concrete - Part 13: Determination of secant modulus of elasticity in compression, Committee European de Normalisation, Brussels, Belgium, 2013.
[35] En 1015–11., Methods of test for mortar for masonry - Part 11: Determination of flexural and compressive strength of hardened mortar, Committee European de Normalisation, Brussels, Belgium, 2019.
[36] Consiglio Superiore del Lavori Pubblici. (2018). Linea Guida per la identificazione, la qualificazione ed il controllo di accettazione di compositi fibrorinforzati a matrice inorganica (FRCM) da utilizzarsi per il consolidamento strutturale di costruzioni esistenti. *In Italian*.
[37] L. Ombres, Analysis of the bond between Fabric Reinforced Cementitious Mortar (FRCM) strengthening systems and concrete, Compos. B Eng, Engineering 69 (2015) 418–426.
[38] A. D'Ambrisi, L. Feo, F. Focacci, Bond-slip relations for PBO-FRCM materials externally bonded to concrete, Compos. B Eng, Engineering 43 (8) (2012) 2938–2949.
[39] Consiglio Nazionale delle Ricerche, CNR DT 215-2018. Istruzioni per la Progettazione, l'Esecuzione ed il Controllo di Interventi di Consolidamento Statico mediante l'utilizzo di Compositi Fibrorinforzati a Matrice Inorganica, 2018. *In Italian.*
[40] L. Lam, J.G. Teng, Stress–strain model for FRP-confined concrete under cyclic axial compression, Engineering Structures 31 (2) (2009) 308–321.
[41] P. Colajanni, M. Fossetti, G. Macaluso, Effects of confinement level, cross-section shape and corner radius on the cyclic behavior of CFRCM confined concrete columns, Construction and Building Materials 55 (2014) 379–389.
[42] L. Lam, J.G. Teng, C.H. Cheung, Y. Xiao, FRP-confined concrete under axial cyclic compression, Cement and Concrete Composites 28 (10) (2006) 949–958.
[43] J. Sakai, K. Kawashima, Unloading and reloading stress–strain model for confined concrete, Journal of Structural Engineering 132 (1) (2006) 112–122.
[44] O. Buyukozturk, T.M. Tseng, Concrete in biaxial cyclic compression, Journal of Structural Engineering 110 (3) (1984) 461–476.
[45] R. Abbasnia, F. Hosseinpour, M. Rostamian, H. Ziaadiny, Cyclic and monotonic behavior of FRP confined concrete rectangular prisms with different aspect ratios, Construction and Building Materials 40 (2013) 118–125.
[46] Y. Shao, Z. Zhu, A. Mirmiran, Cyclic modeling of FRP-confined concrete with improved ductility, Cement and Concrete Composites 28 (10) (2006) 959–968.